Research Article | Vol. 30, No. 2 / 17 Jan 2022 / Optics Express 2539
Optics EXPRESS

Efficient integrated tri-modal coupler for few-mode fibers

JULIAN L. PITA RUIZ,[1,2,3,*] LUCAS G. ROCHA,[1,2] JUN YANG,[4] ŞÜKRÜ EKIN KOCABAŞ,[4] MING-JUN LI,[4] IVAN ALDAYA,[1,5] PAULO DAINESE,[4] AND LUCAS H. GABRIELLI[1,2]

[1] *Photonics Research Center, University of Campinas, Campinas 13083-859, SP, Brazil*
[2] *School of Electrical and Computer Engineering, University of Campinas, Campinas 13083-852, SP, Brazil*
[3] *"Gleb Wataghin" Physics Institute, University of Campinas, Campinas 13083-859, SP, Brazil*
[4] *Corning Research & Development Corporation, One Science Drive, Corning, New York 14830, USA*
[5] *Center for Advanced and Sustainable Technologies, State University of São Paulo, São João da Boa Vista 13876-750, SP, Brazil*
[*] *jpita@unicamp.br*

Abstract: This paper demonstrates a high-efficiency vertical grating coupler for the LP_{01x}, LP_{11ax}, and LP_{11bx} modes of a graded-index few-mode fiber. The coupler is composed of a non-uniform straight bidirectional grating that was inverse-designed to address the desired fiber modes, combined with two mode-selective directional couplers and two tapers. The device was fabricated by e-beam lithography with a minimum feature size of 100 nm and presented coupling efficiencies of −3.0 dB, −3.6 dB, and −3.4 dB for the LP_{01x}, LP_{11ax}, and LP_{11bx} modes, respectively. The high efficiency of the proposed CMOS-compatible coupler demonstrates its potential as a key device for high-capacity networks exploiting space division multiplexing on few-mode fibers.

1. Introduction

The popularization of multimedia applications, in combination with the migration to cloud storage and computing platforms, are commonly claimed as the main factors for the current Internet traffic rise [1,2]. Therefore, telecommunication operators are facing increasing pressure to enhance the performance of their infrastructures [3]. This pressure is particularly critical in large-scale data centers, where energy efficiency is imperative to keep costs low while following the data rates that the market demands [4,5]. In this context, silicon photonics has emerged as the most attractive platform to meet these requirements [6]. Due to the compatibility with CMOS technology, silicon photonics inherits the advantages of its mature manufacturing infrastructure and offers the benefits of delivering compact devices directly integrating optics and microelectronics for efficient signal processing [7,8]. One technique that promises further increases in the data transmission capacity of optical fibers is spatial division multiplexing (SDM): after exploiting time, frequency, and polarization, only the spatial dimension of light remains to be used in the effort to increase transmission rates per fiber [9]. SDM can be implemented either using multi-core or few-mode fibers (FMFs), both of which potentially lead to a significant reduction of the cost per transmitted bit, as the cost of a single laser source is shared among the different spatial channels [10]. In addition, both SDM approaches outperform links based on multiple parallel single-core single-mode fibers not only in terms of capacity but also physical density, which are becoming an increasing concern in state-of-the-art hyper-scale datacenters [11]. Therefore, the integration of SDM techniques with silicon photonics is an important step in the direction of increasing the capacity and efficiency of future optical communication systems, which is why it has been under active development by the scientific community.

#446097 https://doi.org/10.1364/OE.446097
Journal © 2022 Received 18 Oct 2021; revised 17 Dec 2021; accepted 18 Dec 2021; published 11 Jan 2022

Optics EXPRESS

In this sense, a significant effort has been dedicated in recent years to develop either coupling between photonic chips and multi-core fibers [12–15], or different multi-mode devices, such as mode demultiplexers, splitters, and bends [16–18]. The coupling between photonic chips and multi-core fibers has been addressed in several works [12–15]. However, multimode fiber-to-chip couplers are still in their early development stage. Most of the reported multimode couplers are out-of-plane because the in-plane coupling is difficult due to the constraints imposed by the conventional silicon-on-insulator (SOI) platform. In practice, when modes with nodes in the direction orthogonal to the substrate plane are coupled, achieving high efficiency requires either additional layers [19] or complex postprocessing of the chip [20]. Even if out-of-plane couplers typically present lower coupling efficiency than the in-plane devices, the former are not restricted to the edge of the chip and they usually occupy smaller footprint areas [9], both of which contribute to denser device integration. Previous works in FMF coupling [10,21–24] have reported couplers with efficiencies of at least −3.9 dB [22], −5.9 dB [22], −9 dB [10], and −14.3 dB [23], for coupling to 2, 4, 6, and 8 LP modes, respectively.

In this paper, we experimentally demonstrate a 3-mode coupler on a CMOS-compatible SOI platform. The coupler is designed to couple light to/from a fiber oriented in the direction orthogonal to the substrate plane (vertical), which eliminates the need for angled polishing of the fiber and facilitates its alignment. We measured coupling efficiencies of −3.0 dB, −3.6 dB, and −3.4 dB for modes LP_{01x}, LP_{11ax}, LP_{11bx}, respectively, yielding a mode-dependent loss (MDL) of 0.6 dB. These are, to date, the lowest coupling losses presented for an integrated FMF-to-chip coupler that can simultaneously couple up to 3 modes to single-mode integrated waveguides. The presented device can, thus, be employed as mode (de)multiplexer with direct application in SDM. Furthermore, the design could be extended to 6 modes by superimposing two identical straight gratings, as presented in [25]. The rest of the paper is organized as follows: the design process is described and numerically validated in section 2, and in section 3, the fabrication method and the experimental characterization are presented, and finally, in section 4, the paper is concluded.

2. Device design

The device was designed to couple light between an SOI chip with 250 nm device layer thickness, 3 µm buried silicon dioxide layer, and 1 µm silicon dioxide cladding layer, and a FMF. The fiber has graded refractive index that can be described by an alpha profile using:

$$\Delta = \Delta_0 \left[1 - \left(\frac{r}{a}\right)^{\alpha}\right], \tag{1}$$

in which Δ_0 is the maximum relative refractive index change in the center of the core, a is the core radius, and α is the profile shape parameter. For the experimental fiber used in this work, Δ=0.524%, a= 10.3 mm, and α=2.32, thus the fiber supports both the fundamental LP_{01} mode—with a modal field diameter (MFD) of 12.1 µm—and the higher order LP_{11} modes at the operating wavelength of 1550 nm. The coupler consists of a bidirectional nonuniform diffraction grating, two adiabatic tapers, and two identical in-plane modal multiplexers, as illustrated in Fig. 1. The bidirectional grating is used to couple the LP_{01x}, LP_{11ax}, and LP_{11bx} fiber modes into the TE_0 and TE_1 modes of two silicon waveguides with 22 µm × 250 nm cross-section. In particular, LP_{11ax} is evenly coupled to the TE_1 modes of the two multimode output waveguides, whereas LP_{01x} and LP_{11bx} are evenly coupled to the TE_0 modes of the two waveguides with a phase difference of π between them. The two outputs of the bidirectional grating are connected to 930 nm wide input waveguides of the mode-selective directional couplers via 700 µm long linear adiabatic tapers. The length of this taper can be drastically reduced by employing topological optimization as reported in [26]. Each mode-selective directional coupler, based on [27], couples the input TE_0 and TE_1 modes to the fundamental modes of two 450 nm × 250 nm waveguides at their outputs. In summary, the LP_{01x} and the LP_{11bx} modes are directed toward the outputs labeled

Optics EXPRESS

b and c (see Fig. 1) with a phase difference that depends on the mode. The LP_{11ax}, on the other hand, is directed to outputs a and d. The information contained in each mode can be extracted by combining the signals from two outputs: in the case of LP_{11ax}, it is enough to combine outputs a and d in phase. In the cases of LP_{01x} and LP_{11bx}, the separation can be achieved by combining the signals of outputs b and c with a directional coupler, such that, the in-phase and out-of-phase components of the inputs—corresponding, respectively, to LP_{01x} and LP_{11bx}—are separated at the two output ports of the directional coupler. A possible design is depicted in Fig. 1, where the phase shifters employed to ensure constructive interference of the desired mode in each output are included. The figure also shows a zoom-in of the bidirectional nonuniform grating and the position of the FMF, alongside the field profile of the three coupled modes. The section of the device that was fabricated is highlighted by dashed blue lines in Fig. 1. This section includes the bi-directional grating, the tapers, and the mode-selective directional couplers, which represents the original contribution of this work, whereas the design of directional couplers and phase shifters is mature and has been demonstrated in multiple works [28,29]. In order to measure the intensity at the outputs of the two couplers, denoted as a, b, c, and d, single-mode grating couplers were added to the fabricated section.

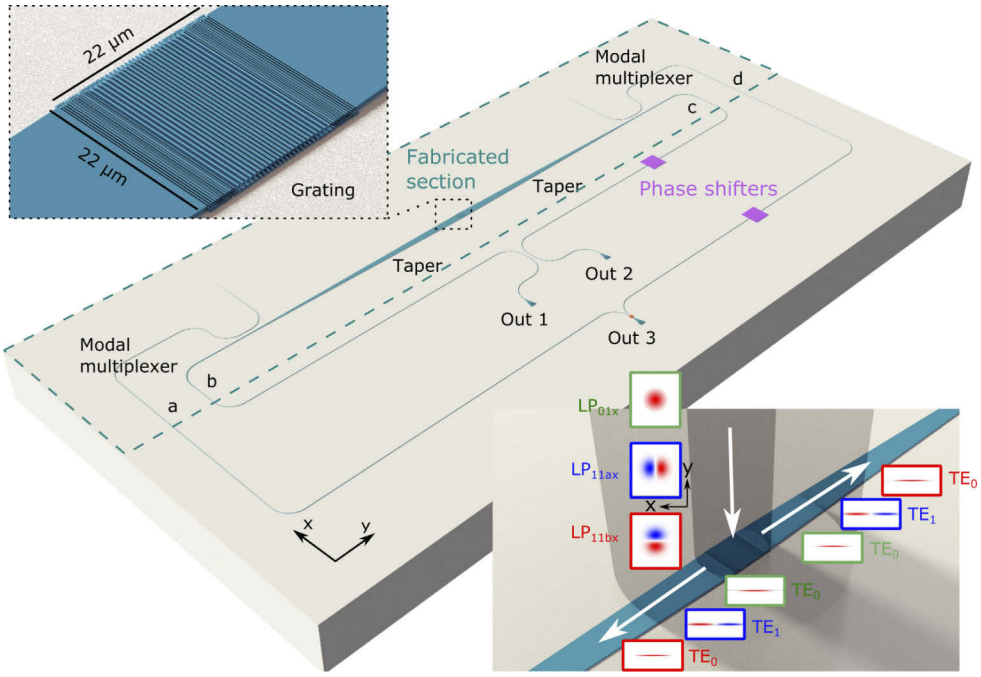

Fig. 1. Schematic of the designed device alongside the FMF. The amplitude profiles of the three coupled modes and a zoom-in of the bidirectional grating are also included. Labels a through d indicate the outputs of the device. In the fabricated prototype, each of those outputs is directly connected to a conventional single-mode grating coupler for independent testing.

The bidirectional grating was optimized using SPINS [30,31] through 2d simulations. A full 3d optimization would require a few weeks to complete, even on a modern workstation. On the other hand, a 2d optimization could be completed in 22 hours, requiring modest computational resources. Due to the symmetry properties of 2d simulations, field variations along the *x* direction are dismissed and therefore 2d designs are restricted to the LP_{01x} and LP_{11bx} modes. However, all three modes have similar effective indices. Furthermore, the field profiles in the *y* direction

Optics EXPRESS

are similar for LP_{11ax} and LP_{01x} modes. As a result, a 2d coupler optimized for LP_{01x} also works for LP_{11ax}, albeit exciting the TE_1 mode of the Si waveguide (LP_{11ax}) as opposed to the TE_0 mode (LP_{01x}). Hence, the error function minimized in the optimization process is described by:

$$\mathcal{E} = \sum_{m=1}^{2} \left(1 - |S_{2m}|^2 - |S_{3m}|^2\right)^2, \tag{2}$$

in which S_{2m} and S_{3m} are the scattering parameters for the LP_{01x} and LP_{11bx} modes at the output of the two waveguides. The optimization was evaluated at a wavelength of 1.55 µm. At this design stage, different etch levels were also considered, with the highest efficiency being attained for an etch depth of 120 nm. Figure 2(a) and Fig. 2(b) show the electric field magnitude within the optimized grating for modes LP_{01x} and LP_{11bx}, respectively, with coupling efficiencies of −1.5 dB and −1.4 dB. After the optimization, the grating efficiency was evaluated by 3d Finite Difference Time Domain (FDTD) simulations, resulting in −2.5 dB, −3.0 dB, and −2.2 dB for the LP_{01x}, LP_{11ax}, and LP_{11bx} modes, respectively, as shown in Fig. 2(c). Those results confirm that the coupling efficiencies for LP_{01x} and LP_{11ax} are indeed similar, justifying the choice of optimizing the structure in 2d. The difference between the 2d and 3d simulation results can be understood by noting that 2d simulation is an approximation that neglects any variations of field and geometry in the x direction (w.r.t. Figure 1).

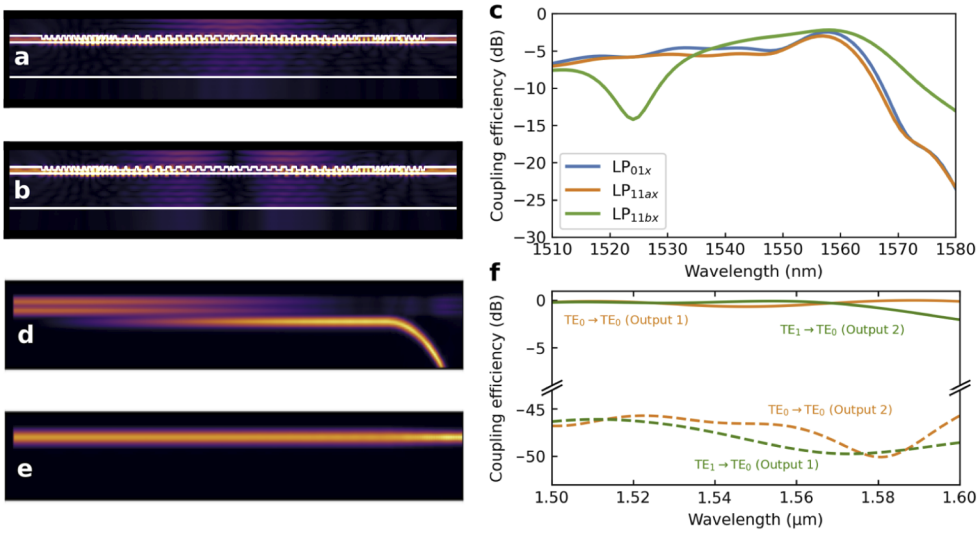

Fig. 2. Simulation results of the constitutive blocks of the multimode coupler. (a) Lateral view of the electric field magnitude for excitation of the LP_{01x} mode in the grating. (b) Analogous to (a) for LP_{11bx}. (c) Coupling efficiencies of the grating for the 3 FMF modes of interest from 3d FDTD simulations. (d) Top view of the electric field magnitude for the TE_1 mode in the in-plane mode multiplexer. (e) Analogous to (d) for the TE_0 mode. (f) Coupling efficiencies and crosstalk (XT) of the in-plane mode multiplexer.

Simulation results for the mode-selective directional coupler used in the device are presented in Fig. 2(d–f). Figure 2(d) shows the top view of the field amplitude for the TE_1 mode, whereas in Fig. 2(e) the field amplitude for TE_0 is represented. The insertion loss for modes TE_0 and TE_1 are, respectively, 0.02 dB and 0.08 dB, both extremely low, with XT between outputs below −45 dB. The wavelength response of the device is flat, with a 3 dB bandwidth exceeding the simulation window of 100 nm.

Optics EXPRESS

3. Fabrication and characterization

The device was fabricated at Applied Nanotools (ANT) rapid fabrication service for silicon photonic integrated circuit prototyping. The silicon patterning was performed using e-beam lithography and reactive ion etching (RIE) with full-depth and (120±10) nm, with a minimal feature size of 100 nm. Covering the chip, a 1 µm silicon dioxide layer was deposited via plasma-enhanced chemical vapor deposition (PECVD). One-half of the fabricated coupler can be seen in the optical microscope image in Fig. 3(a). Scanning electron microscopy (SEM) images also show the details of the mode-selective directional coupler and the bidirectional grating, which occupies a square area of 22 µm × 22 µm. At the ends of the single-mode waveguides coming out of the mode coupler identified as a, b, c, and d in Fig. 1, focused gratings designed for single mode fiber (SMF) with a modal diameter of 10.4 µm are included.

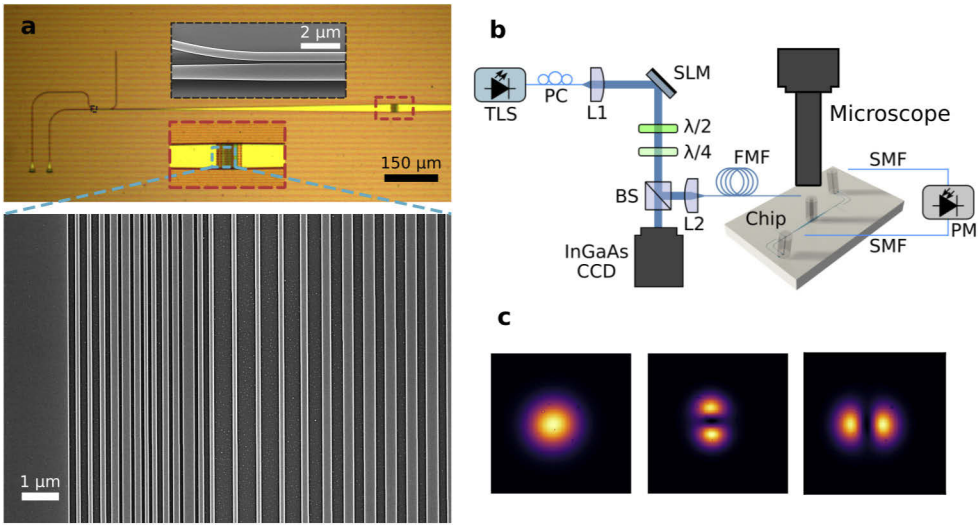

Fig. 3. Fabricated prototype characterization. (a) Optical and SEM images of the fabricated device showing details of the mode-selective directional coupler (top inset) and the grating (bottom). (b) Characterization setup for the prototype with excitation of specific modes in the FMF. (c) Profiles of the excited modes captured by the InGaAs camera.

In order to characterize the fabricated device we employed the setup shown in Fig. 3(b). The polarization of the light emitted by a tunable laser source with an operating wavelength ranging from 1460 nm to 1540 nm is set using a polarization rotator before the collimated beam and directed toward a spatial light modulator (SLM). Different blazed phase masks were imprinted on SLM to independently excite the LP_{01x}, LP_{11ax}, and LP_{11bx} modes of the FMF. The correct alignment and proper excitation of the modes is continuously monitored using an InGaAs camera. In Fig. 3(c) the captured beam profiles are shown. After free-space polarization control based on $\lambda/2$ and $\lambda/4$ plates, the beam is coupled into the FMF, which is aligned to the integrated coupler with the assistance of an optical microscope.

To compute the coupling efficiency of the LP_{01x} mode, we excited this mode at the input of the FMF, measured the powers at ports b and c, added them, normalized with respect to the input power of the mode, and discounted the loss of the single-mode coupler. Afterwards, we excited the LP_{11bx} mode and followed the same process, whereas for the case of LP_{11ax}, we performed a similar process considering the power levels at port a and d instead of b and c. The coupling efficiencies each mode are shown in Fig. 4(a). Maximum coupling efficiencies of −3.0 dB, −3.6 dB, and −3.4 dB were achieved for the LP_{01x}, LP_{11ax}, and LP_{11bx} modes at

Optics EXPRESS

1516 nm, 1515 nm, and 1512 nm, respectively, thus resulting in an MDL of 0.6 dB. The 3 dB operation bandwidth of the coupler is 13 nm for the LP_{01x} mode (narrowest) and 25 nm for LP_{11ax} (widest). The wavelength drift observed in the measurements, compared to the simulation results in Fig. 2, can be attributed to manufacturing errors. In Fig. 4(a), it is also possible to observe a ripple caused by the cavity generated between the fiber and the chip, which is typical in systems with vertical alignment. The ripple was measured to be in the range between 0.2 dB and 0.7 dB over the operation band, leading to a maximum back-reflection level of 4%. Nevertheless, an index-matched adhesive could be used to reduce back-reflection. It is also important to note that, although the efficiencies were measured with the light coming from the fiber to the chip, the reciprocity of the device ensures the same efficiencies in the opposite direction, i.e., for coupling light from the chip to the FMF.

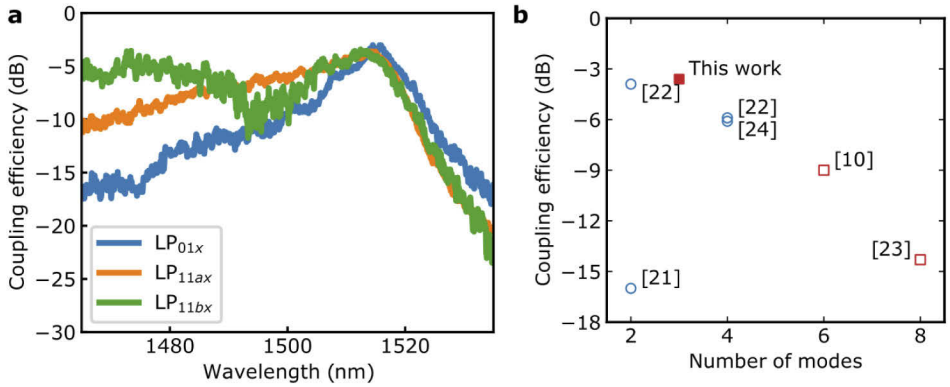

Fig. 4. Experimental results. Measured coupling efficiencies for the LP_{01}, LP_{11ax}, and LP_{11bx} modes. (b) Comparison of the proposed device with previously reported integrated multimode couplers in terms of the number of supported modes and the coupling efficiency. Red squares indicate devices that address the two orientations of LP_{11x} mode.

Figure 4(b) and Table 1 compare the proposed FMF coupler to other works reporting integrated multimode couplers. We observe that, in general, the coupling efficiency tends to decrease as the number of addressed modes increases. In this sense, it is important to note that the proposed device outperforms couplers that address fewer modes, indicating an excellent performance. Furthermore, only [23], [10], and this work are able to couple both orientations of LP_{11x}, meaning LP_{11ax} and LP_{11bx}, which is particularly challenging considering the symmetries of the fiber and conventional gratings. In order to highlight the reported devices that are designed to deal with

Table 1. Comparison of current couplers for FMF. Mode family LP_{11b} is highlighted because of the difficulty in coupling this family.

Reference	MFD (μm)	LP Modes	Efficiency (dB)	Bandwidth (nm)
[21]	11	01x, 11ax	−16.0	NA
[23]	10.7	01x/y, 11ax/y, **11bx/y**, 21ax/y	−14.3[a]	>30
[10]	10	01x/y, 11ax/y, **11bx/y**	−9	31
[24]	15.6	01x/y, 11ax/y	−6.1	15
[22]	11	01x/y, 11ax/y	−5.9	21.6
[22]	11	01x, 11ax	−3.9	59
This work	12.1	01x, 11ax, **11bx**	−3.6	13

[a]Includes the loss of the input single-mode coupler.

Optics EXPRESS

the two orthogonal orientations of LP_{11x} mode, a red square marker is employed in Fig. 4(b) and bold font is used in Table 1.

4. Conclusions

In summary, we have presented and characterized an integrated multimode coupler capable of coupling the modes LP_{01x}, LP_{11ax}, and LP_{11bx} from a FMF to an SOI chip. The combination of an optimized non-uniform bidirectional grating and high-performance modal multiplexers led to coupling efficiencies of −3.0 dB, −3.6 dB, and −3.4 dB for the three coupled modes at 1516 nm, 1515 nm, and 1512 nm, respectively. The challenge of addressing all 6 modes of the FMF (including the *y*-polarized modes) should be achievable, with some penalty added to the efficiencies, by overlapping 2 identical structures at 90°, since the fiber is coupled vertically. Alternatively, a device capable to couple a higher number of modes could be designed by employing multi-objective optimization algorithms. These results indicate the device has great potential to enable the interconnection of SDM systems from fibers to the chip, as it shows an unprecedented coupling efficiency among multimode couplers.

Funding. Coordenação de Aperfeiçoamento de Pessoal de Nível Superior (88881.311020/2018); Fundação de Amparo à Pesquisa do Estado de São Paulo (2015/24517-8, 2016/19270-6, 2018/25339-4); Conselho Nacional de Desenvolvimento Científico e Tecnológico (302036/2018-0, 311035/2018-3, 432303/2018-9).

Acknowledgments. We thank ANT for the fabrication of the samples in a dedicated run. We also thank Paulo F. Jarschel for fruitful discussions and technical assistance.

Disclosures. The authors declare that they have no conflicts of interest.

Data availability. Data underlying the results presented in this paper are not publicly available at this time but may be obtained from the authors upon reasonable request.

References

1. Y. Liu, X. Wei, J. Xiao, Z. Liu, Y. Xu, and Y. Tian, "Energy consumption and emission mitigation prediction based on data center traffic and pue for global data centers," Glob. Energy Interconnect. **3**(3), 272–282 (2020).
2. A. S. Andrae, "New perspectives on internet electricity use in 2030," Eng. Appl. Sci. Lett. **3**(4), 19–27 (2020).
3. R. Lin, Y. Cheng, M. De Andrade, L. Wosinska, and J. Chen, "Disaggregated data centers: Challenges and trade-offs," IEEE Commun. Mag. **58**(2), 20–26 (2020).
4. X. Zhou, R. Urata, and H. Liu, "Beyond 1tb/s datacenter interconnect technology: challenges and solutions," in *2019 Optical Fiber Communications Conference and Exhibition (OFC)*, (IEEE, 2019), pp. 1–3.
5. M.-J. Li, "Novel optical fibers for space division multiplexed transmission systems in data centers," in *2017 Conference on Lasers and Electro-Optics (CLEO)*, (IEEE, 2017), pp. 1–2.
6. A. Rahim, T. Spuesens, R. Baets, and W. Bogaerts, "Open-access silicon photonics: Current status and emerging initiatives," Proc. IEEE **106**(12), 2313–2330 (2018).
7. W. Bogaerts and L. Chrostowski, "Silicon photonics circuit design: methods, tools and challenges," Laser Photonics Rev. **12**(4), 1700237 (2018).
8. M. Teng, A. Honardoost, Y. Alahmadi, S. S. Polkoo, K. Kojima, H. Wen, C. K. Renshaw, P. LiKamWa, G. Li, S. Fathpour, R. Safian, and L. Zhuang, "Miniaturized silicon photonics devices for integrated optical signal processors," J. Lightwave Technol. **38**(1), 6–17 (2020).
9. W. Shi, Y. Tian, and A. Gervais, "Scaling capacity of fiber-optic transmission systems via silicon photonics," Nanophotonics **9**(16), 4629–4663 (2020).
10. T. Watanabe, B. I. Bitachon, Y. Fedoryshyn, B. Baeuerle, P. Ma, and J. Leuthold, "Coherent few mode demultiplexer realized as a 2d grating coupler array in silicon," Opt. Express **28**(24), 36009–36019 (2020).
11. L. Zhang, J. Chen, E. Agrell, R. Lin, and L. Wosinska, "Enabling technologies for optical data center networks: Spatial division multiplexing," J. Lightwave Technol. **38**(1), 18–30 (2020).
12. Y. Ding, F. Ye, C. Peucheret, H. Ou, Y. Miyamoto, and T. Morioka, "On-chip grating coupler array on the SOI platform for fan-in/fan-out of MCFs with low insertion loss and crosstalk," Opt. Express **23**(3), 3292 (2015).
13. L. Gan, J. Zhou, L. Shen, X. Guo, Y. Wang, C. Yang, W. Tong, L. Xia, S. Fu, and M. Tang, "Ultra-low crosstalk fused taper type fan-in/fan-out devices for multicore fibers," in *2019 Optical Fiber Communications Conference and Exhibition (OFC)*, (IEEE, 2019), pp. 1–3.
14. L. G. Rocha, J. L. P. Ruiz, and L. H. Gabrielli, "Compact grating coupler array for multicore fiber fabricated with duv lithography," in *2021 SBFoton International Optics and Photonics Conference (SBFoton IOPC)*, (IEEE, 2021), pp. 1–4.

Optics EXPRESS

15. J. L. P. Ruiz, L. G. Rocha, J. Yang, Ş. E. Kocabaş, M.-J. Li, I. Aldaya, P. Dainese, and L. H. Gabrielli, "Compact dual-polarization silicon integrated couplers for multicore fibers," Opt. Lett. **46**(15), 3649–3652 (2021).
16. J. L. P. Ruiz, A. A. Amad, L. H. Gabrielli, and A. A. Novotny, "Optimization of the electromagnetic scattering problem based on the topological derivative method," Opt. Express **27**(23), 33586–33605 (2019).
17. J. L. P. Ruiz, I. Aldaya, P. Dainese, and L. H. Gabrielli, "Design of compact arbitrary-ratio multimode power splitters based on topological derivative," IEEE Photonics Technol. Lett. **32**(18), 1187–1190 (2020).
18. C. Li, D. Liu, and D. Dai, "Multimode silicon photonics," Nanophotonics **8**(2), 227–247 (2018).
19. D. Dai and M. Mao, "Mode converter based on an inverse taper for multimode silicon nanophotonic integrated circuits," Opt. Express **23**(22), 28376–28388 (2015).
20. J. Zhu, H. Huang, Y. Zhao, Y. Li, Z. Sheng, and F. Gan, "Efficient silicon integrated four-mode edge coupler for few-mode fiber coupling," Chin. Opt. Lett. **20**(1), 011302 (2022).
21. D. Garcia-Rodriguez, J. L. Corral, A. Griol, and R. Llorente, "Bimodal grating coupler design on soi technology for mode division multiplexing at 1550 nm," Opt. Express **26**(15), 19445–19455 (2018).
22. Y. Tong, X. Zhou, Y. Wang, C.-W. Chow, and H. K. Tsang, "Bridging the graded-index few-mode fibre with photonic integrated circuits via efficient diffraction waveguide gratings," in *submitted to European Conference on Integrated Optics*, (2020).
23. Y. Ding and K. Yvind, "Efficient silicon pic mode multiplexer using grating coupler array with aluminum mirror for few-mode fiber," in *2015 Conference on Lasers and Electro-Optics (CLEO)*, (IEEE, 2015), pp. 1–2.
24. Y. Tong, W. Zhou, X. Wu, and H. K. Tsang, "Efficient mode multiplexer for few-mode fibers using integrated silicon-on-insulator waveguide grating coupler," IEEE J. Quantum Electron. **56**(1), 1–7 (2020).
25. T. Watanabe, Y. Fedoryshyn, and J. Leuthold, "2-d grating couplers for vertical fiber coupling in two polarizations," IEEE Photonics J. **11**(4), 1–9 (2019).
26. L. Cheng, S. Mao, Z. Chen, Y. Wang, C. Zhao, and H. Fu, "Ultra-compact dual-mode mode-size converter for silicon photonic few-mode fiber interfaces," Opt. Express **29**(21), 33728–33740 (2021).
27. X. Wu, C. Huang, K. Xu, C. Shu, and H. K. Tsang, "Mode-division multiplexing for silicon photonic network-on-chip," J. Lightwave Technol. **35**(15), 3223–3228 (2017).
28. L. Chrostowski and M. Hochberg, *Silicon photonics design: from devices to systems* (Cambridge University Press, 2015).
29. J. Sun, E. Timurdogan, A. Yaacobi, E. S. Hosseini, and M. R. Watts, "Large-scale nanophotonic phased array," Nature **493**(7431), 195–199 (2013).
30. L. Su, D. Vercruysse, J. Skarda, N. V. Sapra, J. A. Petykiewicz, and J. Vučković, "Nanophotonic inverse design with spins: Software architecture and practical considerations," Appl. Phys. Rev. **7**(1), 011407 (2020).
31. L. Su, R. Trivedi, N. V. Sapra, A. Y. Piggott, D. Vercruysse, and J. Vučković, "Fully-automated optimization of grating couplers," Opt. Express **26**(4), 4023–4034 (2018).